Synthesis and transparent conductivity of crack-free La:BaSnO3 epitaxial flexible sheets

Journal:	*Dalton Transactions*
Manuscript ID	DT-ART-04-2023-001097
Article Type:	Paper
Date Submitted by the Author:	11-Apr-2023
Complete List of Authors:	Gong, Lizhikun; Hokkaido University Yu, Rui; Hokkaido University Ohta, Hiromichi; Hokkaido University, Research Institute for Electronic Science; Hokkaido University Katayama, Tsukasa; Hokkaido University, research institute for electronic science

SCHOLARONE™
Manuscripts

Synthesis and transparent conductivity of crack-free La:BaSnO$_3$ epitaxial flexible sheets

Lizhikun Gong[1], Rui Yu[1], Hiromichi Ohta[2] and Tsukasa Katayama[2,3]*

[1]Graduate School of Information Science and Technology, Hokkaido University, N14W9, Kita, Sapporo 060-0814, Japan

[2]Research Institute for Electronic Science, Hokkaido University, N20W10, Kita, Sapporo 001-0020, Japan

[3]JST-PRESTO, Kawaguchi, Saitama 332-0012, Japan

*Corresponding author: katayama@es.hokudai.ac.jp

1

Abstract

La-doped $BaSnO_3$ (LBSO), which exhibits both high electron mobility and visible-light transparency, is a promising transparent electrode/transistor material that does not require expensive elements such as indium. However, because a high crystal orientation is necessary for high mobility, the development of a synthetic technique is crucial for next-generation optoelectronic applications. One promising method for achieving this is the lift-off and transfer method. Epitaxial films are first deposited on single-crystal substrates, peeled off from the substrates, and subsequently transferred onto other substrates. However, such transferred sheets typically contain a high density of cracks. Therefore, LBSO sheets with flexibility, high mobility, and transparency have not yet been reported. In this study, we successfully synthesized crack-free LBSO epitaxial sheets via a lift-off and transfer method using a water-soluble $Sr_3Al_2O_6$ sacrificial layer and amorphous (a-)Al_2O_3 protection layer. The LBSO sheet simultaneously exhibited a high electron mobility of 80 $cm^2V^{-1}s^{-1}$ and a wide optical bandgap of 3.5 eV owing to the epitaxial crystallinity of the sheet. Moreover, two types of LBSO sheets were prepared, flat and rolled sheets, by tuning the lift-off process. The flat sheet had a lateral size of 5 mm × 5 mm, whereas the rolled sheet had a tube shape with a height of 5 mm and a diameter of 1 mm. Such large crack-free area and flexibility were achieved in LBSO sheets owing to the use of the a-Al_2O_3 protection layer.

1. Introduction

The development of flexible materials with high transparency and conductivity is crucial for next-generation optoelectronic applications such as wearable devices. Conventional flexible transparent conductive materials are mainly limited to ultra-thin metals, [1] nanocarbons (carbon nanotubes and graphene), [2-4] conductive polymers, [5] and amorphous oxide semiconductors.[6-8] However, the investigation of crystallized oxides with high orientation is also important to utilize their unique functionalities such as high Hall mobility. In this study, we focused on crystallized La-doped $BaSnO_3$ (LBSO), which exhibits both visible light transparency and high electron mobility (320 cm^2 V^{-1} s^{-1} in bulk single crystals[9, 10] and 183 cm^2 V^{-1} s^{-1} in epitaxial films[11]). Additionally, because LBSO does not contain rare elements such as indium and it is stable against high temperatures and humidity, it has been actively investigated for the application of electrodes in halide perovskite solar cells. [12] Although flexible amorphous LBSO films do not exhibit high electrical conductivity, we expected that the LBSO epitaxial film, which is peeled off and pasted on a flexible substrate, would simultaneously exhibit high electrical conductivity and flexibility.

The peeling-off and transfer method is promising in the fabrication of flexible oxide single-crystal sheets. The epitaxial oxide film was first fabricated on a water-soluble $Sr_3Al_2O_6$ (SAO) sacrificial layer grown on a $SrTiO_3$ (STO) single-crystal substrate. [14-17] By immersing the epitaxial oxide film in pure water, the oxide sheet can be peeled off from the substrate because the SAO sacrificial layer dissolves in water. Through this method, various types of oxide sheets such as perovskite manganites, [18, 19] $BiFeO_3$, [20] $BaTiO_3$, [21-27] $SrRuO_3$, [28] $SrTiO_3$, [29] and LBSO[30] have been obtained.

However, it is difficult to suppress the generation of cracks in the sheet during the lift-off process. Although Singh *et al.* [30] obtained millimeter-size crack-free LBSO sheets on a Si substrate by precisely tuning the lift-off process, such as changing the material of the sacrificial layer, fabrication of large-area sheets without cracks is extremely difficult because of the epitaxial strain between the LBSO and SAO layers. To overcome this difficulty, we deposited an amorphous (a-)Al_2O_3 protection layer before peeling it off. This method is very effective in suppressing the generation of cracks in the

sheets; therefore, we fabricated crack-free large-area single-crystal oxide sheets used a-Al_2O_3 as protection layer. [31] Herein, we demonstrate the fabrication of crack-free large-size LBSO sheets with high crystallinity and high orientation through the lift-off and transfer method using SAO and a-Al_2O_3 as sacrificial and protection layers, respectively. Two types of LBSO sheets, rolled and flat, were obtained. The rolled sheet had a tubular shape with a height of 5 mm and a diameter of 1 mm, whereas the lateral size of the flat sheet was 5 mm × 5 mm. A significantly large crack-free area was achieved owing to the use of an a-Al_2O_3 protection layer. The difference in curvature between the rolled and flat sheets was as large as 2 mm^{-1}, indicating a high potential for flexible properties of LBSO sheets. LBSO sheets exhibit a wide optical bandgap (3.5 eV) and a higher Hall mobility (80 cm^2 V^{-1} s^{-1}) than other transparent conducting oxide (TCO) films grown on glass, such as indium tin oxide (ITO), Al-doped ZnO, and F-doped SnO_2. [6-8]

2. Experiment

The as-grown films consisting of a-Al_2O_3/LBSO/SAO trilayers were first deposited on $SrTiO_3$(001) single-crystal substrates through pulsed laser deposition (PLD). As the PLD target of the LBSO layer, a $La_{0.02}Ba_{0.98}SnO_{3-\delta}$ ceramic target was synthesized by pre-sintering a mixture of La_2O_3, $BaCO_3$, and SnO_2 powders at 1350 ℃ and sintering the pellet at 1400 ℃. The $Sr_3Al_2O_6$ ceramic target was synthesized by pre-sintering a mixture of $SrCO_3$ and Al_2O_3 powders at 1350 ℃ and sintering the pallet at 1350 ℃. During film deposition, the substrate temperature, oxygen pressure, laser fluence, and laser frequency were precisely controlled at 850 ℃, 10^{-3} Pa, 0.5 J cm^{-2} $pulse^{-1}$, and 2 Hz for the SAO layer; 750 ℃, 20 Pa, 2 $Jcm^{-2}pulse^{-1}$, and 10 Hz for the LBSO layer; and room temperature, 10^{-3} Pa, 2 $Jcm^{-2}pulse^{-1}$, and 10 Hz for the a-Al_2O_3 layer, respectively. The thicknesses of the a-Al_2O_3, LBSO, and SAO layers were 300, 300, and 20 nm, respectively.

The a-Al_2O_3/LBSO layers were peeled from the STO substrate by dissolving the SAO layer in pure water. The as-grown films were placed in pure water for 24 h using two different methods, as illustrated in Figure 1. In the first method, the as-grown film was immersed in pure water with the substrate side facing down. In the second method, the surface of the as-grown film was attached to an

4

adhesive-coated polyethylene terephthalate (PET) substrate before being immersed in pure water. Thereafter, the as-grown PET-attached film was immersed in pure water. Adhesive-coated PET substrates were purchased from Kimoto Co., Ltd. (Prosave UV). The thickness and adhesive force of the PET substrates were 100 μm and 14.8 N/25 mm, respectively.
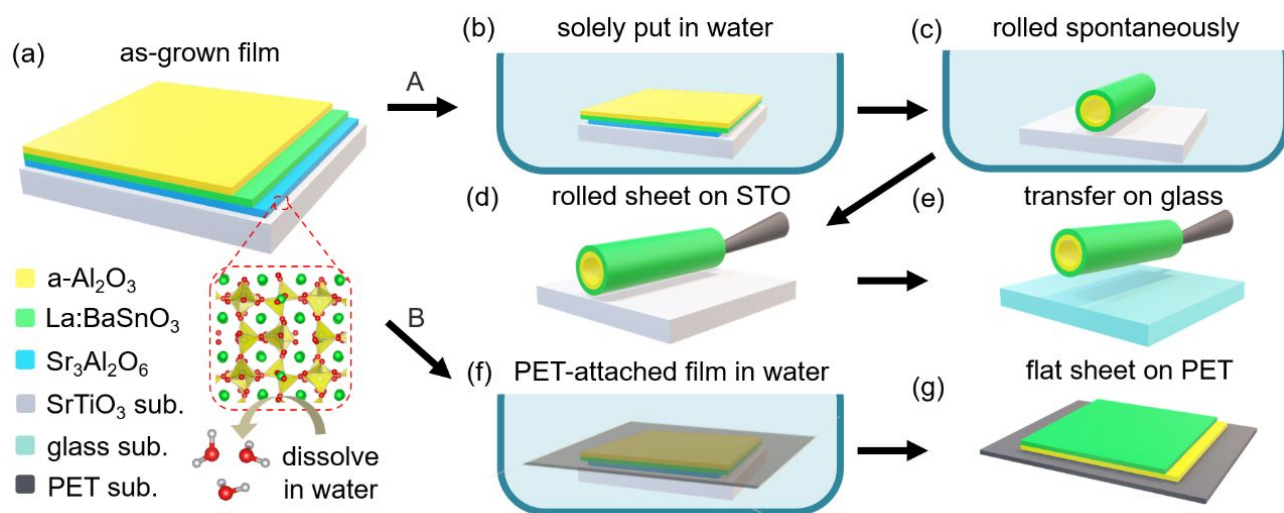

Figure 1. Schematics of the synthesis process of the sheets. (a) As-grown film, (b) the film in pure water, rolled sheet on STO substrate in (c) water and (d) air, (e) rolled sheet transferred onto glass. (f) PET-attached as-grown film in pure water, and (g) flat sheet on PET.

The crystal structures of the as-grown films and obtained sheets were evaluated using X-ray diffraction (XRD) measurements (ATX-G, Rigaku Co.). The surface morphology of the sheets was determined through atomic force microscopy (AFM) measurements (Nanocute, Hitachi High-Tech Science Corp.). The optical transmission and reflectivity spectra of the sheets were measured using an optical spectrophotometer (SolidSpec-3700, Shimadzu Corp.). The conductivity and Hall mobility of the sheets were determined using the conventional four-probe DC method with a van der Pauw electrode configuration.

3. Results and discussion

The as-grown film of the a-Al$_2$O$_3$/LBSO/SAO trilayer was immersed in pure water with the

substrate side facing down for 24 h (Figure 1(b)). The SAO layer started to dissolve in pure water from the edge and completely dissolved after approximately 2 h. Thereafter, the a-Al$_2$O$_3$/LBSO bi-layer was peeled off from the substrate and rolled spontaneously in pure water (Figure 1(c)). Hereafter, the bi-layer sheet is referred to as a LBSO sheet. The rolled LBSO sheet was still attached to the STO substrate owing to van der Waals forces. When the substrate was picked from pure water using tweezers without turning it upside down, the rolled LBSO sheet could also be picked up together with the substrate (Figure 1(d)). The rolled LBSO sheet can be transferred to other substrates such as glass using a sharp needle and tweezers as follows (Figure 1(e)): (1) stick the needle into the hole of the rolled LBSO sheet, (2) lift it up, (3) move it on another substrate, and (4) pull the needle out of the hole of the rolled sheet. Figure 2(a) shows the top and lateral views of the rolled LBSO sheet transferred onto glass. The rolled LBSO sheet had a tubular shape with a height of 5 mm and a diameter of 1 mm. The curvature of the rolled LBSO sheet was as large as 2 mm^{-1}, which is significantly larger than that previously reported for LBSO.[30] The surface of the tube is an LBSO layer. The tubular shape of the rolled LBSO sheet indicates that the in-plane lattice constant of the LBSO layer increased upon the removal of the SAO layer.
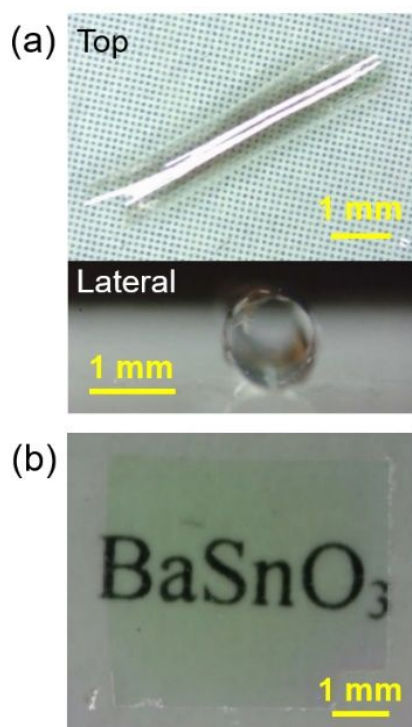
Figure 2. (a) Top and lateral view photographs of the rolled LBSO sheet transferred onto glass and (b) photograph of the flat LBSO sheet on the PET substrate.

A flat LBSO sheet was also prepared. Figures 1(f–g) illustrate the synthesis of the flat sheet. The surface of the as-grown film was first attached to an adhesive-coated PET substrate (Figure 1(f)). Thereafter, the PET-attached as-grown film was immersed in pure water for 24 h. After the SAO sacrificial layer was dissolved in pure water, the STO substrate was peeled from the surface of the sheet. The LBSO sheet remained flat on the PET substrate (Figure 1(g)) because the adhesive force of the PET substrate was significantly stronger than the van der Waals force between the sheet and STO substrate. Figure 2(b) shows a photograph of the flat LBSO sheet on the PET substrate. No cracks were observed on the sheet. A. Gustavo *et al* reported high crack resistance properties of Al_2O_3-containing glasses.[32] They fabricated xAl_2O_3–$(1-x)SiO_2$ glasses ($x = 0.3–0.6$) and found that the glass cracking resistance increased with increasing x; especially, the $x = 0.6$ glass exhibited the highest indentation cracking resistance, elastic moduli, and hardness in the binary system.[32] The authors proposed that the local structure around aluminum atoms play a key role in the increased cracking resistance through shear deformation processes.[32] In this study, we further increased the aluminum content and used a-Al_2O_3 as protection layer, resulting in crack-free LBSO sheet. The lateral size of the sheet was 5 mm × 5 mm, which was larger than that of a previously reported LBSO sheet (2 mm × 5 mm). [30]

Figure 3(a) shows the out-of-plane XRD pattern of the as-grown films. The 001 and 002 diffraction peaks of LBSO were clearly observed along with the 008 diffraction peak of SAO (inset of Figure 3(a)). The full width half maximum of the rocking curve for the SAO 008 diffraction peak is 2.8° (Fig. S1). Figure S2 shows the reciprocal space map (RSM) around the STO 103 diffraction peak of the as-grown film. A spot-like 103 diffraction peak was also observed for LBSO. These results indicate that the LBSO layer was heteroepitaxially grown on the SAO layer. This is because the crystal structure of SAO, particularly the arrangement of Sr ions, is similar to that of the perovskite structure, as illustrated in Figure 1. The in-plane and out-of-plane lattice constants (*a* and *c*, respectively) of the LBSO layer in the as-grown film were determined as 4.11 and 4.135 Å, respectively. In comparison

with bulk $BaSnO_3$ (a = 4.116 Å), [10] the LBSO layer in the as-grown film has a shorter a but longer c, indicating that the LBSO layer is under compressive strain from the SAO layer. This is reasonable because $a/4$ of bulk SAO ($a/4$ = 3.961 Å) is shorter than the a of bulk $BaSnO_3$. As shown in Figure 2(a), the tubular shape of the rolled LBSO sheet indicates that the in-plane lattice constant of the LBSO layer increased upon the removal of the SAO layer. The increase in the in-plane lattice constant is due to the release of the compressive strain in the LBSO layer by peeling off from the SAO/STO substrate.
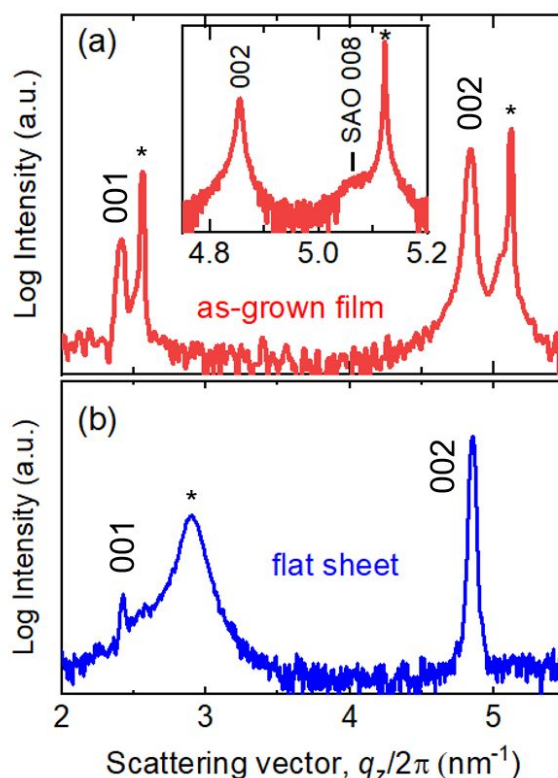

Figure 3. Out-of-plane XRD patterns of (a) the as-grown film and (b) flat LBSO sheet on the PET substrate. Asterisks correspond to the STO or PET substrates.

Figure 3(b) shows the out-of-plane XRD pattern of the flat LBSO sheet on PET. The 001 and 002 diffraction peaks of LBSO were still observed, indicating that the crystallographic orientation was maintained throughout the sheet synthesis process. However, the 008 diffraction peak of SAO disappeared because the SAO layer dissolved in pure water. The 001 and 002 diffraction peaks of LBSO shifted to the higher-angle side, whereas the c value decreased to 4.123 Å. This is derived from the release of in-plane compressive lattice strain from the substrate by removing the SAO layer. The

8

intensity ratio of the 001 to 002 diffraction peaks of the flat LBSO sheet was 0.84%, which is almost equal to that of bulk $BaSnO_3$ (1.2%) and the as-grown film (0.96%) (Figure 3(a)).

The crystallinity of the flat LBSO sheet was evaluated using rocking curve measurements of the 002 diffraction peaks (Figure 4(a)). The full width at half maximum of the rocking curve was 0.6°, which was wider than that of the as-grown film (0.2°), indicating that crystallinity decreased during the sheet synthesis process. We speculate that the in-plane lattice constant of the LBSO layer increases slightly owing to the release of the in-plane compressive lattice strain from the substrate, resulting in an in-plane lattice distortion. Figure 4(b) shows the AFM results for the flat LBSO sheet. The root mean square of the surface roughness is 0.9 nm, indicating that the surface of the sheet is not coarse.
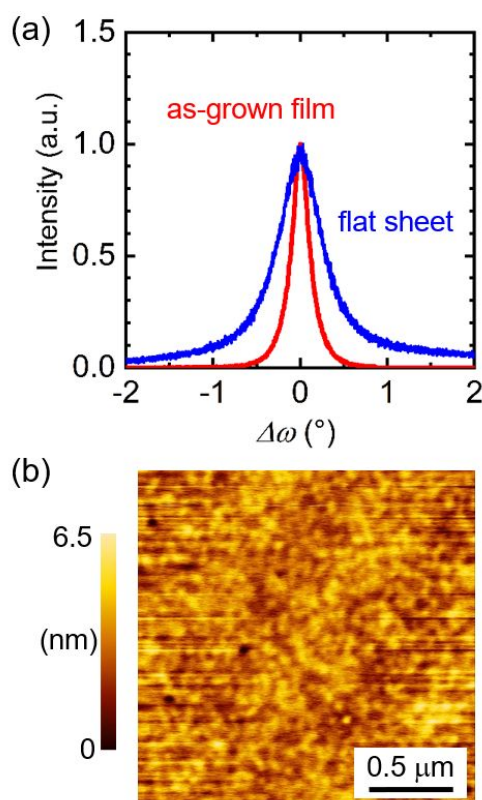

Figure 4. (a) Rocking curves of the 002 diffraction peak of the as-grown film and flat LBSO sheet. (b) AFM image of the flat LBSO sheet.

Next, we discuss the optical properties of the flat LBSO sheets. Figure 5(a) shows the optical transmission and reflection spectra as functions of wavelength. In the visible light region, at a

wavelength range of 380–780 nm, the transmission value was higher than 73%, indicating the visible light transparency of the LBSO sheet. The optical bandgap of the flat LBSO sheet was estimated from the Tauc plot of the $(\alpha h v)^2$–hv curve, where α denotes the absorption coefficient and hv is the photon energy. The optical bandgap (E_g) of the LBSO sheet was 3.5 eV, which was almost equal to that of bulk LBSO single crystals (3.5 eV) [9] and LBSO epitaxial films on MgO substrates (3.55 eV). [33]
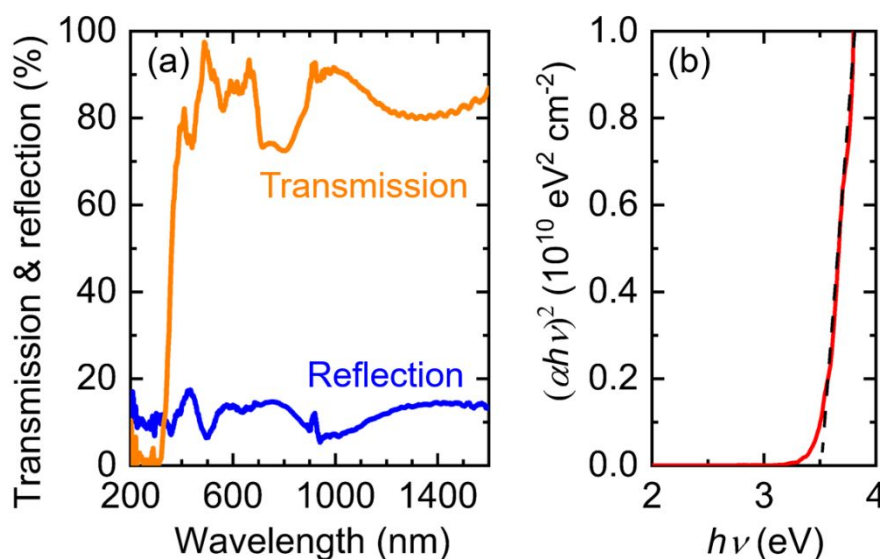

Figure 5. (a) Optical transmission and reflection spectra as functions of wavelength, and (b) photon energy dependence of $(\alpha h v)^2$ of the flat LBSO sheet.

Figure 6 shows the temperature (T) dependence of the electrical conductivity (σ) of the flat LBSO sheet. The σ value increased with decreasing T, indicating that the flat LBSO sheet was a degenerated semiconductor. Similar behavior was also observed in LBSO films on SrTiO$_3$ and MgO substrates. [34, 35] The σ value and Hall mobility (μ) of the flat LBSO sheet at 300 K were 1.9×10^3 S/cm and 80 cm^{2}V^{-1}s^{-1}, respectively. The Hall mobility was slightly lower than that of the LBSO film on the STO substrate (96 cm^{2}V^{-1}s^{-1}) [36] because of the lower crystallinity of the sheet (Figure 4(a)). According to a previous study, LBSO films grown on mica substrates also exhibit flexibility. [37] However, σ of the LBSO film on the mica substrate was one order of magnitude lower ($\sigma = 140$ S/cm) than that of the flat LBSO sheet, [37] indicating significantly lower electron mobility of the LBSO film on the mica substrate. In comparison to other TCOs grown on glass, such as ITO ($E_g = 3.6$ eV, $\mu = 54$

cm^{2}V^{-1}s^{-1}),[7] Al-doped ZnO (E_g = 3.0 eV, μ = 46 cm^{2}V^{-1}s^{-1}),[8] and F-doped SnO$_2$ (E_g = 4.3 eV, μ = 15 cm^{2}V^{-1}s^{-1}),[6] the LBSO sheet (E_g = 3.5 eV, μ = 80 cm^{2}V^{-1}s^{-1}) exhibits higher electron mobility. In addition to TCOs, graphene[4] and carbon nanotubes[3] are also promising candidates for fabricating transparent electrodes. However, they tend to suffer from instability at the edges, restricting their potential applications.[38] Silver colloids have also garnered considerable attention owing to their high transparency and mobility,[39] although it is still necessary to improve their particle size consistency and reproducibility.[40] LBSO has several advantages, including stability against high temperature and humidity, does not use expensive elements such as indium, and high transparency and mobility, which demonstrate its high potential for optoelectronic applications.
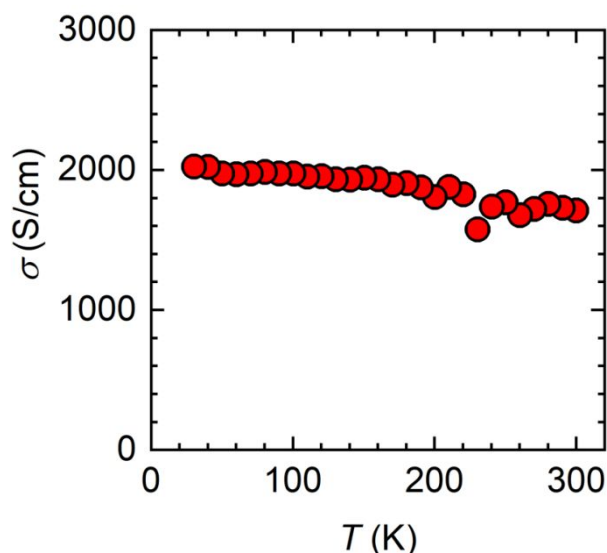

Figure 6. Temperature dependence of the electrical conductivity of the flat LBSO sheet.

4. Conclusion

In this study, we successfully obtained large-size rolled and flat crack-free LBSO sheets through a lift-off and transfer method using a water-soluble SAO layer and a-Al$_2$O$_3$ protection layer. The rolled sheet had a tubular shape with a height of 5 mm and a diameter of 1 mm, whereas the lateral size of the flat sheet was 5 mm × 5 mm. The significantly large crack-free area was achieved because of the presence of the a-Al$_2$O$_3$ protection layer. The difference in curvature between the rolled and flat sheets was as large as 2 mm^{-1}, indicating the excellent flexibility of the LBSO sheets. The LBSO sheet

exhibited a wide E_g of 3.5 eV and high Hall mobility of 80 cm^{2}V^{-1}s^{-1}, demonstrating high potential for next-generation optoelectronic device applications.

Supporting Information

See supporting information for the details of RSM of the as-grown film and sheet.

Acknowledgments

References

1.   J. Bernède, L. Cattin, M. Morsli and Y. Berredjem, Ultra-thin metal layer passivation of the transparent conductive anode in organic solar cells, *Sol. Energy Mater. Sol. Cells*, 2008, **92**, 1508-1515.

2.   J. Kwak, J. H. Chu, J.-K. Choi, S.-D. Park, H. Go, S. Y. Kim, K. Park, S.-D. Kim, Y.-W. Kim and E. Yoon, Near room-temperature synthesis of transfer-free graphene films, *Nat. Commun.*, 2012, **3**, 645.

3.   L.-M. Peng, Z. Zhang and S. Wang, Carbon nanotube electronics: recent advances, *Mater. Today*, 2014, **17**, 433-442.

4.   X. Huang, Z. Zeng, Z. Fan, J. Liu and H. Zhang, Graphene‐based electrodes, *Adv. Mater.*, 2012, **24**, 5979-6004.

5.   D. Kumar and R. Sharma, Advances in conductive polymers, *Eur. Polym. J.*, 1998, **34**, 1053-1060.

6.   H. Kim, R. Auyeung and A. Piqué, Transparent conducting F-doped SnO2 thin films grown by pulsed laser deposition, *Thin Solid Films*, 2008, **516**, 5052-5056.

7.   O. Tuna, Y. Selamet, G. Aygun and L. Ozyuzer, High quality ITO thin films grown by dc and RF sputtering without oxygen, *J. Phys. D: Appl. Phys.*, 2010, **43**, 055402.

8.   S. Cornelius, M. Vinnichenko, N. Shevchenko, A. Rogozin, A. Kolitsch and W. Möller, Achieving high free electron mobility in ZnO: Al thin films grown by reactive pulsed magnetron sputtering, *Appl. Phys. Lett.*, 2009, **94**, 042103.

9.   H. J. Kim, U. Kim, T. H. Kim, J. Kim, H. M. Kim, B.-G. Jeon, W.-J. Lee, H. S. Mun, K. T. Hong and J. Yu, Physical properties of transparent perovskite oxides (Ba, La) SnO$_3$ with high electrical mobility at room temperature, *Phys. Rev. B*, 2012, **86**, 165205.

10.   H. J. Kim, U. Kim, T. H. Kim, H. S. Mun, B.-G. Jeon, K. T. Hong, W.-J. Lee, C. Ju, K. H. Kim and K. Char, High mobility in a stable transparent perovskite oxide, *Appl. Phys. Express*, 2012, **5**, 061102.

11.   H. Paik, Z. Chen, E. Lochocki, A. Seidner H, A. Verma, N. Tanen, J. Park, M. Uchida, S. Shang and B.-C. Zhou, Adsorption-controlled growth of La-doped BaSnO3 by molecular-beam epitaxy, *Apl Mater.*, 2017, **5**, 116107.

12.   S. S. Shin, E. J. Yeom, W. S. Yang, S. Hur, M. G. Kim, J. Im, J. Seo, J. H. Noh and S. I. Seok, Colloidally prepared La-doped $BaSnO_3$ electrodes for efficient, photostable perovskite solar cells, *Science*, 2017, **356**, 167-171.

13.   G. Dong, S. Li, M. Yao, Z. Zhou, Y.-Q. Zhang, X. Han, Z. Luo, J. Yao, B. Peng and Z. Hu, Super-elastic ferroelectric single-crystal membrane with continuous electric dipole rotation, *Science*, 2019, **366**, 475-479.

14.   D. Lu, D. J. Baek, S. S. Hong, L. F. Kourkoutis, Y. Hikita and H. Y. Hwang, Synthesis of freestanding single-crystal perovskite films and heterostructures by etching of sacrificial water-soluble layers, *Nat. Mater.*, 2016, **15**, 1255-1260.

15.   D. Lu, S. Crossley, R. Xu, Y. Hikita and H. Y. Hwang, Freestanding Oxide Ferroelectric Tunnel Junction Memories Transferred onto Silicon, *Nano Lett.*, 2019, **19**, 3999-4003.

16.   D. Li, C. Adamo, B. Y. Wang, H. Yoon, Z. Chen, S. S. Hong, D. Lu, Y. Cui, Y. Hikita and H. Y. Hwang, Stabilization of $Sr_3Al_2O_6$ Growth Templates for Ex Situ Synthesis of Freestanding Crystalline Oxide Membranes, *Nano Lett.*, 2021, **21**, 4454-4460.

17.   S. S. Hong, M. Gu, M. Verma, V. Harbola, B. Y. Wang, D. Lu, A. Vailionis, Y. Hikita, R. Pentcheva and J. M. Rondinelli, Extreme tensile strain states in $La_{0.7}Ca_{0.3}MnO_3$ membranes, *Science*, 2020, **368**, 71-76.

18.   C. Jin, Y. Zhu, X. Li, F. An, W. Han, Q. Liu, S. Hu, Y. Ji, Z. Xu and S. Hu, Super‐Flexible Freestanding $BiMnO_3$ Membranes with Stable Ferroelectricity and Ferromagnetism, *Adv. Sci.*, 2021, **8**, 2102178.

19.   Q. Lu, Z. Liu, Q. Yang, H. Cao, P. Balakrishnan, Q. Wang, L. Cheng, Y. Lu, J.-M. Zuo and H. Zhou, Engineering Magnetic Anisotropy and Emergent Multidirectional Soft Ferromagnetism in Ultrathin Freestanding $LaMnO_3$ Films, *ACS nano*, 2022, **16**, 7580-7588.

20.   R. Guo, L. You, W. Lin, A. Abdelsamie, X. Shu, G. Zhou, S. Chen, L. Liu, X. Yan, J. Wang and J. Chen, Continuously controllable photoconductance in freestanding $BiFeO_3$ by the macroscopic flexoelectric effect, *Nat. Commun.*, 2020, **11**, 2571.

21.   H. Sun, J. Wang, Y. Wang, C. Guo, J. Gu, W. Mao, J. Yang, Y. Liu, T. Zhang and T. Gao, Nonvolatile ferroelectric domain wall memory integrated on silicon, *Nature communications*, 2022, **13**, 1-9.

22.   Y. Zhou, C. Guo, G. Dong, H. Liu, Z. Zhou, B. Niu, D. Wu, T. Li, H. Huang and M. Liu, Tip-Induced In-Plane Ferroelectric Superstructure in Zigzag-Wrinkled $BaTiO_3$ Thin Films, *Nano Lett.*, 2022, **22**, 2859-2866.

23.   Q. Wang, H. Fang, D. Wang, J. Wang, N. Zhang, B. He and W. Lü, Towards a Large-Area Freestanding Single-Crystal Ferroelectric $BaTiO_3$ Membrane, *Crystals*, 2020, **10**, 733.

24.   M. Lee, J. R. Renshof, K. J. van Zeggeren, M. J. Houmes, E. Lesne, M. Šiškins, T. C. van

Thiel, R. H. Guis, M. R. van Blankenstein and G. J. Verbiest, Ultrathin Piezoelectric Resonators Based on Graphene and Free‐Standing Single‐Crystal $BaTiO_3$, *Adv. Mater.*, 2022, **34**, 2204630.

25.   G. Dong, Y. Hu, C. Guo, H. Wu, H. Liu, R. Peng, D. Xian, Q. Mao, Y. Dong and Y. Zhao, Self‐Assembled Epitaxial Ferroelectric Oxide Nanospring with Super‐Scalability, *Adv. Mater.*, 2022, **34**, 2108419.

26.   Y. Zhao, R. Peng, Y. Guo, Z. Liu, Y. Dong, S. Zhao, Y. Li, G. Dong, Y. Hu, J. Zhang, Y. Peng, T. Yang, B. Tian, Y. Zhao, Z. Zhou, Z. Jiang, Z. Luo and M. Liu, Ultraflexible and Malleable Fe/$BaTiO_3$ Multiferroic Heterostructures for Functional Devices, *Adv. Funct. Mater.*, 2021, **31**, 2009376.

27.   T. Wang, R. C. Peng, W. Peng, G. Dong, C. Zhou, S. Yang, Z. Zhou and M. Liu, 2‐2 Type PVDF‐Based Composites Interlayered by Epitaxial (111)‐Oriented BTO Films for High Energy Storage Density, *Adv. Funct. Mater.*, 2022, **32**, 2108496.

28.   K. Gu, T. Katayama, S. Yasui, A. Chikamatsu, S. Yasuhara, M. Itoh and T. Hasegawa, Simple Method to Obtain Large‐Size Single‐Crystalline Oxide Sheets, *Adv. Funct. Mater.*, 2020, **30**, 2001236.

29.   R. Xu, J. Huang, E. S. Barnard, S. S. Hong, P. Singh, E. K. Wong, T. Jansen, V. Harbola, J. Xiao and B. Y. Wang, Strain-induced room-temperature ferroelectricity in $SrTiO_3$ membranes, *Nat. Commun.*, 2020, **11**, 1-8.

30.   P. Singh, A. Swartz, D. Lu, S. S. Hong, K. Lee, A. F. Marshall, K. Nishio, Y. Hikita and H. Y. Hwang, Large-Area Crystalline $BaSnO_3$ Membranes with High Electron Mobilities, *ACS Appl. Electron. Mater.*, 2019, **1**, 1269-1274.

31.   L. Gong, M. Wei, R. Yu, H. Ohta and T. Katayama, Significant Suppression of Cracks in Freestanding Perovskite Oxide Flexible Sheets Using a Capping Oxide Layer, *ACS nano*, 2022, **16**, 21013-21019.

32.   Rosales-Sosa, G. A.; Masuno, A.; Higo, Y.; Inoue, H. Crackresistant, $Al_2O_3-SiO_2$ glasses. Sci. Rep. 2016, **6**, 23620.

33.   Q. Liu, F. Jin, J. Dai, B. Li, L. Geng and J. Liu, Effect of thickness on the electrical and optical properties of epitaxial $(La_{0.07}Ba_{0.93})SnO_3$ thin films, *Superlattices Microstruct.*, 2016, **96**, 205-211.

34.   A. V. Sanchela, M. Wei, H. Zensyo, B. Feng, J. Lee, G. Kim, H. Jeen, Y. Ikuhara and H. Ohta, Large thickness dependence of the carrier mobility in a transparent oxide semiconductor, La-doped $BaSnO_3$, *Appl. Phys. Lett.*, 2018, **112**, 232102.

35.   A. V. Sanchela, T. Onozato, B. Feng, Y. Ikuhara and H. Ohta, Thermopower modulation clarification of the intrinsic effective mass in transparent oxide semiconductor $BaSnO_3$, *Phys. Rev. Mater.*, 2017, **1**, 034603.

36.   A. V. Sanchela, M. Wei, J. Lee, G. Kim, H. Jeen, B. Feng, Y. Ikuhara, H. J. Cho and H. Ohta, Buffer layer-less fabrication of a high-mobility transparent oxide semiconductor, La-doped $BaSnO_3$, *J. Mater. Chem. C*, 2019, **7**, 5797-5802.

37.   W. Sun, J. Fan, R. Xu, X. Zhang, C. Kan, W. Liu, L. Zhang, C. Ma, D. Hu and Y. Ji, High optical transmittance and anomalous electronic transport in flexible transparent conducting

oxides $Ba_{0.96}La_{0.04}SnO_3$ thin films, *Ceram. Int.*, 2018, **44**, 18001-18006.

38.   Ç. O. Girit, J. C. Meyer, R. Erni, M. D. Rossell, C. Kisielowski, L. Yang, C.-H. Park, M. Crommie, M. L. Cohen and S. G. Louie, Graphene at the edge: stability and dynamics, *Science*, 2009, **323**, 1705-1708.

39.   M. Wu, S. Yu, L. He, L. Yang and W. Zhang, High quality transparent conductive Ag-based barium stannate multilayer flexible thin films, *Sci. Rep.*, 2017, **7**, 103.

40.   I. Pastoriza-Santos and L. M. Liz-Marzán, Colloidal silver nanoplates. State of the art and future challenges, *J. Mater. Chem.*, 2008, **18**, 1724-1737.